Horizontal transfer of a preneoplastic phenotype depends upon tunneling nanotubes and BMP signaling.

Cristina Cuella Martin[1,2,3], Thanh Thuy Nguyen *[1,2,3], Alexia Bertin *[1,2,3], Kevin Geistlich[1,2,3,4], Boris Guyot[1,2,3], Sylvain Lefort[1,2,3], Emmanuel Delay[1,2,3,4], Charline Dalverny[3,5], Alice Boissard[6], Cécile Henry[6], François Guillonneau[6,7,8], Eve-Isabelle Pécheur §*[1,2,3] and Véronique Maguer-Satta §*[1,2,3,4]

1. CNRS UMR5286, Centre de Recherche en Cancérologie de Lyon, 69008 Lyon, France;
2. Inserm U1052, Centre de Recherche en Cancérologie de Lyon, 69008 Lyon, France;
3. Université Claude Bernard Lyon 1, Lyon, France;
4. Centre Léon Bérard, 69008 Lyon, France;
5. Centre Technologique des Microstructures (CTμ), 69622 Villeurbanne, France;
6. Prot'ICO proteomics facility, Institut de Cancérologie de l'Ouest, 49055 Angers, France,
7. Nantes Université, Inserm, CNRS, CRCI2NA, U1307, UMR6075, 44000 Nantes, France;
8. Equipe Labellisée Ligue Contre le Cancer, Paris, France.

* These authors contributed equally; § Co-corresponding authors

Co-corresponding authors: Eve-Isabelle PÉCHEUR and Véronique MAGUER-SATTA, Centre de Recherche en Cancérologie de Lyon-CRCL, UMR CNRS 5286/Inserm U1052, 28 rue Laënnec, 69373 Lyon Cedex 08, France; 33-4-7878-2907 or 33-4-7878-2806.
Emails: eve-isabelle.pecheur@inserm.fr ; veronique.maguer-satta@lyon.unicancer.fr

Keywords: Tunneling nanotubes, cell communication, preneoplasia, BMP, luminal breast tumor initiation, stem cells.

Abstract.

Tunneling nanotubes (TNTs) are thin, actin-rich structures that facilitate long-distance intercellular communication through the transfer of molecules and organelles. While their role in cancer progression is well-established, their involvement in the earliest stages of tumor initiation remains unexplored. Using normal human mammary primary cells, a model of early luminal breast transformation, and mammary organoids, we demonstrate that TNTs become increasingly abundant and elongated during the initial phases of luminal breast cell transformation. Notably, these structures preferentially connect transformed donor cells to non-transformed acceptor cells, establishing a directional horizontal communication network. Unbiaised proteomic analyses and (correlative) super-resolution microscopy reveal that, through this network, transformed cells transfer key molecular signals - including the Bone Morphogenetic Protein receptor type 1b (BMPR1b) - to non-transformed acceptor cells, inducing rapid changes of their proteome landscape. Functional analyses of acceptor cells reveal changes in levels of transcripts and phenotypic alterations, including the acquisition of anchorage-independent growth—a hallmark of preneoplastic progression.

Our findings highlight how TNT-mediated transfer initiates a BMP-dependent cascade of molecular and phenotypic changes in acceptor cells, effectively propagating a preneoplastic state within the luminal breast epithelium. By elucidating these early events, we provide novel insights into the mechanisms underlying the onset and spread of BMP-mediated epithelial transformation in luminal breast cancer, offering new avenues for understanding how preneoplastic states emerge and disseminate within the tissue microenvironment.

With 2.3 million women affected worldwide and 700,000 deaths per year, breast cancer is the leading cause of cancer-related death in women, with luminal types representing 70% of all cases [1], and ductal carcinoma *in situ* (DCIS) the earliest non-invasive stage. The Bone Morphogenetic Proteins (BMP) pathway is a key actor altered during luminal breast tumorigenesis [2–4]. Together with an interleukin-6 (IL6)-mediated inflammation, enhanced BMP2 secretion by the niche surrounding mammary stem cells fuels their transformation into cancer stem cells *via* amplification of their response to the kinase BMP receptor type 1b (BMPR1b), without detectable genetic alterations [3,5]. Cancer stem cells can drive tumorigenesis and chemoresistance through exogenous signaling pathways that maintain their stemness and promote survival [6,7]. BMPR1b-silenced transformed mammary cells have drastically decreased capacities to initiate tumor formation *in vivo* [3]. However, the early dynamics of BMP-mediated transformation and the evolution of non-transformed mammary cells towards tumor cells remain unexplored.

Tunneling nanotubes (TNTs) are thin, transient actin-based structures enabling long-range intercellular communication [8,9], *via* the transfer of organelles, small molecules, proteins and nucleic acids. TNTs have been implicated in tumor progression, metastasis, and chemoresistance. Cancer cells linked to neurons by TNTs exhibited enhanced metastatic capacities [10–12]. Yet the role of TNTs at earliest stages of tumorigenesis is unknown.

While BMPs and TNTs have independently been associated with breast cancer, their potential interaction is unexplored. Also, the nature, directionality, and functional consequences of cell/cell communications at the tumor initiation stage remain ill-defined.

In this work, we aimed to delineate the interplay between the BMP pathway and TNT-mediated communication, to shed light on the earliest steps of transformation of (immature) mammary cells.

75 **Results.**

76 **TNT formation during mammary epithelial stem cells transformation.**

77 Early BMP-driven transformation dynamics was explored by using our MCF10A-derived stem
78 cell models obtained by chronic exposure to IL6 and BMP2 (MC26 and M1B26; Fig. 1A) [3,5].
79 Sorting of BMPR1b-expressing cells prior to cytokine treatment, followed by soft agar clones
80 selection, led to quicker establishment of transformed cells (M1B26), with greater *in vitro*
81 anchorage-independent growth and *in vivo* engraftment than in non BMPR1b-sorted cells
82 (MC26). These models display DCIS molecular features and robustly recapitulate the *in vivo*
83 BMP pathway alterations (*3, 5)*. Super-resolution Airyscan confocal microscopy observations
84 of non-transformed control (MCF10A-CT) and transformed cells (MC26, M1B26) revealed
85 long-range contacts *via* long thin F-actin-rich TNTs [13] (Fig. 1B). Although TNT quantification
86 requires low-confluence cultures [14], long-range TNTs were also detectable at high cell density
87 (Fig. S1A). Transformed cells exhibited over twice as many TNTs as non-transformed cells
88 (Fig. 1C, left). The proportion of long TNTs increased ~fivefold with transformation (Fig. 1C,
89 right). However, TNT average length did not differ between cell lines (Fig. S1B). Neither TNT
90 number nor length varied in non-transformed cells exposed to conditioned medium of
91 transformed ones (Fig. S1B-D). TNTs in transformed cells were often branched, with
92 ramifications and bulges (Fig. 1D black arrow) [8,13]. While most TNTs were open-ended,
93 allowing a cell-cell cytoplasmic continuum (Fig. 1E), some close-ended TNTs featuring a Gap
94 junction at one tip were seen (Fig. S1E). TNTs did not adhere to the substrate and were observed
95 within 3D structures such as acini, basic functional units of breast glandular tissue (Fig. 1F;
96 Fig. S1F). TNTs also contained microtubules [8,15] (Fig. S1G), and mitochondria [16] (Fig. 1G; Fig.
97 S1H). Importantly, transformed cells could also establish TNT connections with non-
98 transformed primary fibroblasts (Fig. 1H) and epithelial mammary cells (Fig. 1I) isolated from
99 healthy human breast samples.

100 This indicates that early mammary cell transformation leads to an enhanced ability of
101 transformed cells to connect to their neighbors through TNTs.

102

103 **Directional transfer of cellular material *via* TNTs from transformed to non-transformed**
104 **cells.** To investigate how TNTs connect cells, we cocultured mCherry-expressing MCF10A-CT
105 with GFP-expressing M1B26 cells, seeded at low density [14]. Both M1B26 transformed (Tf) and
106 MCF10A-CT non-transformed (NoTf) cells formed TNT structures, connecting Tf to Tf, NoTf
107 to NoTf and Tf to NoTf cells (Fig. 2A). Quantification of TNT contacts revealed that
108 connections were more frequent and abundant from Tf towards NoTf cells than in the opposite

direction (Fig. 2B,C). Fluorescent material from GFP-tagged Tf cells accumulated within the cytoplasm of NoTf cells (Fig. 2D), suggesting a directional transfer *via* TNTs, Tf cells as donors and NoTf cells as acceptors (Fig. 2E; Movie S1; Fig. S2A). To assess the proportion of cellular exchange between cells, mCherry-NoTf cells were cocultured with GFP-Tf cells for 8 days. Flow cytometry analysis revealed a higher proportion of mCherry-NoTf cells exhibiting green fluorescence uptake compared to GFP-Tf cells acquiring red fluorescence (Fig. S2B), indicating a preferential Tf-to-NoTf directional transfer (Fig. 2F-H). Switching fluorophores between Tf and NoTf cells yielded similar results (Fig. S2C,D), and this directional transfer increased over time (Fig. S2E-I). When using normal human primary mammary cells as NoTf cell sources, we also observed a Tf-to-NoTf directional material transfer in coculture (Fig. 2J,K), as with MCF10A-CT cells (Fig. S2J). To evaluate the contribution of cell-cell communication through secretion of soluble compounds and extracellular vesicles, we performed cultures of normal human primary cells: (i) with Tf cells separated by a physical barrier (Transwell™), to impede TNT formation; (ii) in Tf cells conditioned medium (CM, schematic Fig. 2I). In the former condition, the number of acceptor cells dropped in both transfer directions (Fig. 2J,K; Fig. S2J). In the latter, no fluorescence exchange *via* soluble components was observed (Fig. S2K,L). Therefore, directional material transfer preferentially occurs *via* TNTs from Tf to NoTf cells, and rather than through other forms of cell-cell communication.

TNT-mediated transfer modulates proteomic features of acceptor cells.

Fluorescently-labeled cells cultured for 8 days (Fig. 3A), were sorted by flow cytometry into four populations: non-transformed (NoTf), transformed (Tf), non-transformed cells that received fluorescent material (NoTf accept), and non-transformed cells from the same coculture that did not receive any material (NoTf no accept). Unbiased proteomic screening of each population followed by gene enrichment pathway analysis revealed that most enriched pathways in NoTf accept, compared to NoTf no accept of the same coculture, were related to transport (organic/nitrogen compounds, protein, transmembrane, intracellular), and to localization of intracellular organelles, macromolecules and proteins (Fig. 3B). Other pathways pointed to mitochondrion organization and activity. Volcano plot analysis revealed that NoTf accept were statistically distinct from NoTf no accept cells of the same coculture, and from NoTf in monoculture (Fig. 3C; Fig. S3A). Of note, the most overexpressed proteins in the former phenotype were involved in lipid metabolism and transport (*ATP8B1, RAB6B, CES1* – EST1, *MEST*, *PIGA*), intracellular membrane and secretory vesicle trafficking (*RAB6B,*

RAB11B, SYT8, CAV2, TMEM167A), cell growth and morphology maintenance (*TRIQK*), membrane protrusion formation (*ATP8B1*) and actin filament bundling (*LCP1* – Plastin-2) (Table S1). Other overexpressed proteins were linked to mitochondrial activities (*COX7C*, *MALSU1*), possibly related to the presence of mitochondria within TNTs (Fig. 1G; Figs. S1H, S3B).

Six proteins, EST1, Plastin-2, Rab-6B, TRIQK, MEST and MASU1, were markedly overexpressed in NoTf accept compared to NoTf no accept cells from same cocultures (Fig. 3D; Fig. S3C). Corresponding RNA levels were also enhanced in Tf compared to NoTf cells (Fig. S3D). The TNT-mediated transfer of material therefore induces in acceptor cells transcriptional and translational upregulation of key actors involved in progression towards a transformed-like phenotype. This aligns with the downregulation of DAP1 (*DAP*) and thymosin β-10 (*TMSB10*), respectively involved in ribosome hibernation and actin polymerization inhibition (Table S1).

When TNT formation was physically impeded, acceptor cells showed phenotypic differences compared to those in direct coculture (Table S2), but remained comparable to NoTf cells in monoculture (Fig. S3E,F). Notably, NoTf accept cells from direct cocultures exhibited a higher expression of early inflammatory markers (*SERPINA3, CD14*) and motility-related genes (*IGFBP6*) than their Transwell™ counterparts. These findings indicate that TNT-mediated direct contacts with transformed cells induce profound changes in the proteomic landscape of non-transformed acceptor cells, similar to those observed in early transformed cells.

Ras-driven oncogenic transformation being a well-established process, we next investigated whether it could also promote the formation of TNTs. Proteomics revealed a marked increase in H-Ras and K-Ras oncoproteins in NoTf accept cells compared to NoTf cells in monoculture (Fig. 3E). We then examined two additional models involving Ras-mediated transformation of mammary epithelial cells. First, in the Weinberg's model of human mammary epithelial cells immortalized with SV40-L antigen and hTERT, then transformed with H-Ras [17], TNTs were present in malignant and non-malignant cells, with shorter TNTs in the former (Fig. 3F,H). Second, in H-Ras-transformed immature MCF10A-derived AT1 and DCIS cells, malignant cells exhibited fewer TNTs than non-malignant ones, without length difference (Fig. 3G,I). Hence, Ras-induced transformation does not enhance long-distance TNT-mediated communication, contrary to inflammation- and BMP-driven mechanisms relevant to luminal breast cancer clinical occurrence [3].

TNT-mediated transfer impacts the BMP pathway of recipient cells.

Since transmembrane and protein transports were the most impacted processes (Fig. 3B), and given that the BMP pathway is a key driver of luminal transformation [3,4] (Fig. S4A,B), we examined whether this pathway was affected in non-transformed acceptor cells. We focused on the canonical SMAD cascade, and among non-canonical MAPK downstream cascades, on p38 (MAPK14), because the p-p38/p38 ratio exhibited the highest level of expression in Tf cells (Fig. S4A,B). Eight target or regulator proteins of these cascades were extracted from our proteomic screening (Table S3), and assessed for their expression across sorted cell populations post-TNT connections (Fig. 3A). Several proteins involved in the BMP pathway — including ID1, Nup214 [18], spartin, and USP15 [19] — were consistently up- or down-regulated in NoTf acceptor cells, reaching levels comparable to those observed in Tf cells, exclusively after TNT transfer (Fig. 4A). ATF2, a transcription regulator positioned at the BMP pathway/p38 cascade interface, was underexpressed in NoTf acceptor cells, at levels comparable to those in Tf cells. Components of the p38 cascade were markedly altered following TNT-mediated transfer: MAPKAPK2, a kinase activated by p38 phosphorylation, was underexpressed in NoTf acceptor cells, consistent with the role of p38 inhibition in facilitating mammary tumorigenesis [20]. Conversely, Rac1—part of a complex involved in actin bundling and stabilization, regulated by p38—was overexpressed in NoTf cells that received material *via* TNTs (Fig. 4A). BMPR1b expression increased with transformation, and the receptor was localized within TNTs, particularly in bulges, in normal human primary and model mammary cells (Fig. 4B). This was concomitant to the activation of both canonical p-SMAD1/5/8 / SMAD1/5/8, and non-canonical p-p38/p38 and p-ERK/ERK cascades (Fig. S4A,B). Correlative light (scanning) electron microscopy (CLEM) enables to distinguish intra- from extra-cellular epitopes by overlaying optical and scanning electron images of the same region. Airyscan confocal imaging revealed a continuum of BMPR1b in cell bodies, as well as in or on TNTs. However, electron microscopy did not reveal any extracellular BMPR1b epitopes at TNTs (Fig. 4C). This suggests an extracellular localization in the cell body and an intraluminal presence in TNTs, consistent with BMPR1b trafficking through/within TNTs. Although incomplete (Fig. 4D,E top), *BMPR1b* silencing in Tf cells drastically reduced TNT number, and abolished the formation of long TNTs (Fig. 4E bottom). Silencing of G protein-coupled estrogen receptor 1 (*GPER*) was used as control, since no report linked GPER to TNT formation/function. Though more efficient than *BMPR1b* silencing (Fig. 4E top), *GPER* knockdown had no effect on TNT number or length (Fig. 4D,E bottom). Therefore, BMPR1b contributes to the formation and elongation of (long) TNTs.

210 The four sorted cell populations (Figs. 3A, 4F) were then analyzed for BMPR1b mRNA
211 expression. It was found ~8-fold higher in NoTf accept cells previously connected *via* TNTs,
212 compared to an only ~2-fold increase when TNT formation was blocked (Fig. 4G). This
213 supports a role for a TNT-mediated activation of the BMP pathway.
214 These findings underscores the activation of the BMP pathway in NoTf cells acceptor of
215 material from Tf cells, *via* TNT-mediated transfer.
216
217 **After TNT contact with transformed donor cells, non-transformed acceptor cells become**
218 **sensitized to a transforming microenvironment.**
219 Long-term impact of TNT cell-cell horizontal communication was assessed on sorted cells,
220 cultured for up to 16 weeks in the absence or presence BMP2/IL6, mimicking *in vivo* luminal
221 breast tumor conditions (*2)* (Fig. 4F). BMPR1b protein levels rose between weeks 6 and 10
222 before stabilizing, in NoTf accept cells exposed to cytokines after sorting (Fig. 5A left),
223 reaching the highest expression among all populations by week 14 (Fig. 5A right; Fig. S4C,D).
224 Accordingly, p-SMAD1/5/8 / SMAD1/5/8 and p-p38/p38 cascades were activated upon 4 to 6
225 week-exposure to BMP2/IL6 in NoTf accept cells (Fig. 5B,C; Fig. S4E,F). While the SMAD
226 cascade did not return to baseline over weeks (Fig. 5B), the p38 cascade, after a strong
227 activation as early as 4 weeks with cytokines post-sorting, reached baseline levels after 10
228 weeks (Fig. 5C).
229 We then cross-referenced our proteomic and transcriptomic datasets [5], and identified three
230 tumor-associated genes significantly upregulated during transformation: *HOXB6* [21], *CCND2* [22],
231 and *EREG* [23] (Fig. 5D). Their mRNA levels were increased in NoTf acceptor cells connected
232 through TNTs with Tf cells, compared to NoTf cells in monoculture, and to NoTf acceptor cells
233 for which TNT formation was blocked (Fig. 5E). This supports the notion that TNT-mediated
234 transfer may promote a shift towards a preneoplastic state. HoxB6, Cyclin D2 and (pro)-
235 epiregulin protein levels also tended to increase with transformation (Fig. S5A). *HRAS* was
236 overexpressed in NoTf acceptor cells, further substantiating a shift towards a preneoplastic
237 status (Fig. 4E). However, *HRAS* was neither involved in TNT formation, nor in TNT-mediated
238 preneoplastic switch of acceptor cells (Fig. 3F-I). As a negative control, we selected *UFM1*, a
239 gene involved in endoplasmic reticulum stress, a cellular insult suggested to contribute to TNT
240 development [24]. *UFM1* transcript levels remained unchanged regardless of transformation
241 status or material uptake (Fig. S5B,C), indicating that although ER stress may be present, it is
242 not a key driver of the cellular behavior described here.

243 NoTf acceptor cells grown with cytokines up to 16 weeks post-TNT transfer and sorting (Fig.
244 S6A), displayed anchorage-independent growth at earlier time points than other types of sorted
245 cells, and with a number of clones obtained comparable to that of Tf cells (Fig. 5F; Fig. S6B).
246 Potential cross-contamination between Tf and NoTf sorted cell samples was ruled out based on
247 the specific fluorescence of derived soft agar clones (Fig. S6C). All these features are hallmarks
248 of a preneoplastic transformation, observed exclusively in cells that had established TNT
249 contacts with transformed cells prior to sorting, enabling the transfer of transforming
250 information.
251 Hence, these findings unravel the key role of TNT-mediated transfer of transforming cues,
252 including BMPR1b, in driving a preneoplastic switch in previously non-transformed cells
253 receiving material from transformed cells. This TNT communication would prime non-
254 transformed cells to respond to a tumor-promoting microenvironment, ultimately contributing
255 to the propagation of transformation (Fig. 5G).
256

Discussion

Our findings reveal that TNT-mediated transfer of transforming cues from transformed to non-transformed cells activates the BMP signaling pathway in acceptor cells, sensitizing them to a tumor-promoting microenvironment and initiating early features of transformation. The TNT-mediated transfer of mitochondria from stromal to cancer (stem) cells has been well documented [25], and recently, TNTs were shown to enhance the metastatic capacity of cancer cells in primary tumors, receiving mitochondria from neurons [10].

In contrast, the delivery of material from transformed cells to non-transformed neighbors, remains unexplored at very early stages of transformation. Our study is the first to investigate the functional impact of TNT-mediated material exchange between cells of identical phenotype (i.e. epithelial cells), on the predisposition of non-transformed cells to adopt a preneoplastic status. Although donor-to-acceptor material transfer through secretion of soluble compounds and extracellular vesicles occurred, it remained low to negligible, indicating that the processes mainly relied on physical TNT-mediated communications. This horizontal directional transfer from transformed to non-transformed cells leads within days to the overexpression of tumor-related genes and of BMPR1b itself, evocative of a possible feedback loop that maintains transforming conditions (Fig. 5G). Non-transformed cells also undergo profound changes of their proteomic landscape, linked to transport processes, and within weeks acquire phenotypic traits of preneoplasia, such as anchorage-independent growth, sustained BMPR1b overamplification and related mounting of a non-canonical signaling cascade. The earliest events, within one week, comprised the overexpression of tumor-related genes such as *HOXB6*, *CCND2* and *EREG* by non-transformed acceptor cells, after TNT contacts with transformed (donor) cells. Interestingly, upregulation of these genes upon transformation has already been linked to other cancers: (i) *HOXB6*, encoding a homeobox domain-containing transcription factor involved in development, is upregulated in acute myeloid leukemia and osteosarcoma [21,26], with a possible role in cancer initiation [27]; (ii) *CCND2*, encoding cyclin D2, involved in DNA replication, cell division and cell cycle regulation, was dysregulated in gastric, thyroid and colorectal cancers [28], and its overexpression in breast cancer promotes MAPK-mediated cell proliferation and tumor growth [22,29]; (iii) upregulation of *EREG,* encoding the secreted protein ligand of the EGF receptor (EGFR) epiregulin, is linked to breast cancer progression and resistance to tamoxifen by EGFR activation [23,30].

288 Following TNT material transfer, including BMPR1b, *BMPR1B* becomes overexpressed in
289 acceptor cells within a week. The receptor molecule was detected within TNTs, overexpressed
290 in transformed cells, and structurally contributing to TNT elongation. As BMP receptors are
291 known to be located in lipid rafts, BMPR1b could induce TNT formation *via* its interaction with
292 these microdomains [31], from which TNTs might arise [32,33]. These cholesterol-rich microdomains
293 provide high curvature and elasticity necessary for membrane deformation linked to TNT
294 formation. Cholesterol levels together with lipid rafts increase upon transformation, as
295 evidenced in prostate and breast cancer cell lines [34], further substantiated by our proteomic data
296 with acceptor cells displaying enhanced expression of EST1, a carboxylesterase hydrolyzing
297 cholesterol esters into free cholesterol. Additionally, BMP2 was reported to promote actin
298 polymerization via PI3Kα activation [35]. We herein observed that *LCP1* was upregulated upon
299 transformation, concomitantly to its protein Plastin-2, in acceptor cells following TNT transfer.
300 Plastin-2 is a key actin-bundling protein involved in the formation of cellular protrusions [36],
301 overexpressed in epithelial-derived cancers including breast [37]. Its overexpression correlated
302 with cancer cell migration, invasion, metastasis [38] and chemoresistance [39]. Plastin-2 activation
303 depends on serine 5 phosphorylation *via* ERK/MAPK, PI3K, and PKA/PKC pathways,
304 enabling its recruitment to actin filaments and promoting bundling and protrusion elongation,
305 as shown in breast carcinoma [40]. This agrees with findings from the Zurzolo's group, showing
306 that TNT induction by Eps8 involves its actin-bundling activity [41]. Altogether, this might
307 explain the higher number of TNTs observed upon transformation.

308 At the functional level, the analysis of sorted acceptor cells which received material from TNT
309 transfer, revealed their gradual transformation over weeks, faster and more extensively than
310 non-acceptor cells, concomitant to a progressive but sustained activation of the BMP pathway.
311 This induced an initial burst of p38 downstream response, followed by the prolonged activation
312 of the canonical SMAD cascade, only observed when TNT contacts existed. These recipient
313 cells then exhibited preneoplastic traits. Experiments on TNT-forming capacities of mammary
314 cell models, where transformation of either normal primary [17] or MCF10A cells [42] is « switched
315 on » by the H-Ras oncoprotein, showed fewer and shorter TNTs connecting cells. *HRAS* is
316 overexpressed in invasive breast tumors, but the prevalence of *HRAS* mutations in luminal types
317 is negligible [1,43]. These mammary models do not faithfully recapitulate the earliest stages of
318 non-invasive luminal breast tumors triggered, for example, by exposure to carcinogenic cues
319 such as environmental pollutants, endocrine disruptors or alcohol [3,44–46].

320 Here, we unveil for the first time that TNTs transport BMPR1b and propagate transforming
321 cues, in the context of luminal breast cancer initiation. Such processes sensitize acceptor cells
322 to BMP2 signals of the microenvironment, rapidly triggering a cascade of molecular events that
323 culminate in phenotypic changes, with anchorage-independent growth of previously non-
324 transformed cells (Fig. 5G). Combined with the recent demonstration that TNTs can transfer
325 material *in vivo* [47], our work provides the foundation for a new concept: the propagation,
326 through TNTs, of a preneoplastic state within a population of initially non-transformed
327 mammary cells. This process could precede the development of luminal-type tumors, and
328 identify BMPR1b as a major early contributor of the BMP-dependent preneoplastic switch of
329 acceptor cells.

330

Data availability statement. The mass spectrometry proteomics data have been deposited to the ProteomeXchange Consortium via the PRIDE (https://www.ebi.ac.uk/pride/) [48,49] partner repository, with the dataset identifier PXD060023. Transcriptomic data have been deposited on the Gene Expression Omnibus repository, GSE18673411.

Acknowledgements. We thank P. Battiston-Montagne, M. Gautier and C. Vanbelle (CRCL, platform PIC), and D. Ressnikoff (SFR Santé Lyon Est, CIQLE). We thank the "AniRA lentivectors production facility" from the CELPHEDIA Infrastructure and SFR Biosciences, UAR3444/CNRS, US8/Inserm, ENS de Lyon, UCBL, especially G. Froment, D. Nègre and C. Costa. We thank J. Brocard, head of the LYMIC-PLATIM UAR 3444 / US8 microscopy platform (ENS Lyon, Univ Lyon 1), and E. Chatre. We thank B. Manship for english proofreading, P. Mehlen, P. Juin, R. Tomasini, C. Vérollet and B. Bartosch for inspiring discussions. Some illustrations were created in https://BioRender.com.
This work was supported by Agence Nationale de la Recherche (VMS, ANR-10-LABX-0061, ANR-CESA-018-04 and Convergence PLAsCAN ANR-17-CONV-0002); Ligue Nationale contre le Cancer (CCM, doctoral grant), Dept Ain, Rhône (VMS), Saône et Loire (EIP) ; Fondation ARC (CCM, 4th year doctoral grant; VMS, SFI20111203500, PJA20171206331) ; the ERiCAN program of Fondation MSD-Avenir (VMS/EIP, DS-2018-0015) and Associations [Déchaîne Ton Cœur (VMS); Ruban Rose Prix Avenir 2021 (VMS) ; Comité féminin pour le dépistage du cancer du sein 74 (VMS) ; Symatese Fondation (VMS), and Fondation pour la Recherche Médicale (équipe FRM EQU202203014695 VMS).

Contributions: V.M.S. and E-I.P designed and supervised the study, conceived methodological developments and acquired funding. V.M.S. provided administrative support. C.C.M., S.L. and B.G. collaborated in study design, contributed to methodological developments and data interpretations. K.G. performed RNA-seq and proteomic bioinformatic data analyses, and statistical gene-expression analyses. C.C.M., T.T.N., A.B. and E-I.P. performed and interpreted the experiments. C.D. designed and performed SEM and CLEM microscopy experiments. F.G., A.B. and C.H. performed proteomic analyses, and F.G. interpreted proteomic data. E.D. provided primary breast samples, and assisted with their processing. C.C.M., V.M.S and E-I.P. wrote the manuscript. All authors reviewed the manuscript and approved the final version for publication.

Competing interests. The authors declare no competing interests.

References.

1. Cancer Genome Atlas Network. Comprehensive molecular portraits of human breast tumors (2012). Nature *490*, 61–70. https://doi.org/10.1038/nature11412.

2. Zabala, M., Lobo, N.A., Antony, J., Heitink, L.S., Gulati, G.S., Lam, J., Parashurama, N., Sanchez, K., Adorno, M., Sikandar, S.S., et al. (2020). LEFTY1 Is a Dual-SMAD Inhibitor that Promotes Mammary Progenitor Growth and Tumorigenesis. Cell Stem Cell *27*, 284-299.e8. https://doi.org/10.1016/j.stem.2020.06.017.

3. Chapellier, M., Bachelard-Cascales, E., Schmidt, X., Clément, F., Treilleux, I., Delay, E., Jammot, A., Ménétrier-Caux, C., Pochon, G., Besançon, R., et al. (2015). Disequilibrium of BMP2 levels in the breast stem cell niche launches epithelial transformation by overamplifying BMPR1B cell response. Stem Cell Rep. *4*, 239–254. https://doi.org/10.1016/j.stemcr.2014.12.007.

4. Jiang, W.-J., Zhou, T.-H., Huang, H.-J., Li, L.-S., Tan, H., Zhang, R., Wang, Q.-S., and Feng, Y.-M. (2025). Breast Cancer Subtype–Specific Organotropism Is Dictated by FOXF2-Regulated Metastatic Dormancy and Recovery. Cancer Res. *85*, 644–659. https://doi.org/10.1158/0008-5472.CAN-24-0479.

5. Guyot, B., Clément, F., Drouet, Y., Schmidt, X., Lefort, S., Delay, E., Treilleux, I., Foy, J.-P., Jeanpierre, S., Thomas, E., et al. (2023). An Early Neoplasia Index (ENI10), Based on Molecular Identity of CD10 Cells and Associated Stemness Biomarkers, is a Predictor of Patient Outcome in Many Cancers. Cancer Res. Commun. *3*, 1966–1980. https://doi.org/10.1158/2767-9764.CRC-23-0196.

6. Ju, F., Atyah, M.M., Horstmann, N., Gul, S., Vago, R., Bruns, C.J., Zhao, Y., Dong, Q.-Z., and Ren, N. (2022). Characteristics of the cancer stem cell niche and therapeutic strategies. Stem Cell Res. Ther. *13*, 233. https://doi.org/10.1186/s13287-022-02904-1.

7. Bayik, D., and Lathia, J.D. (2021). Cancer stem cell-immune cell crosstalk in tumour progression. Nat. Rev. Cancer *21*, 526–536. https://doi.org/10.1038/s41568-021-00366-w.

8. Resnik, N., Erman, A., Veranič, P., and Kreft, M.E. (2019). Triple labelling of actin filaments, intermediate filaments and microtubules for broad application in cell biology: uncovering the cytoskeletal composition in tunneling nanotubes. Histochem. Cell Biol. *152*, 311–317. https://doi.org/10.1007/s00418-019-01806-3.

9. Rustom, A., Saffrich, R., Markovic, I., Walther, P., and Gerdes, H.-H. (2004). Nanotubular highways for intercellular organelle transport. Science *303*, 1007–1010. https://doi.org/10.1126/science.1093133.

10. Hoover, G., Gilbert, S., Curley, O., Obellianne, C., Lin, M.T., Hixson, W., Pierce, T.W., Andrews, J.F., Alexeyev, M.F., Ding, Y., et al. (2025). Nerve-to-cancer transfer of mitochondria during cancer metastasis. Nature *644*, 252–262. https://doi.org/10.1038/s41586-025-09176-8.

11. Pinto, G., Brou, C., and Zurzolo, C. (2020). Tunneling Nanotubes: The Fuel of Tumor Progression? Trends Cancer *6*, 874–888. https://doi.org/10.1016/j.trecan.2020.04.012.

12. Vignais, M.-L., Caicedo, A., Brondello, J.-M., and Jorgensen, C. (2017). Cell Connections by Tunneling Nanotubes: Effects of Mitochondrial Trafficking on Target Cell Metabolism, Homeostasis, and Response to Therapy. Stem Cells Int. *2017*, 6917941. https://doi.org/10.1155/2017/6917941.

13. Huang, L., Zhang, J., Wu, Z., Zhou, L., Yu, B., Jing, Y., Lin, D., and Qu, J. (2022). Revealing the structure and organization of intercellular tunneling nanotubes (TNTs) by STORM imaging. Nanoscale Adv. *4*, 4258–4262. https://doi.org/10.1039/d2na00415a.

14. Sáenz-de-Santa-María, I., Henderson, J.M., Pepe, A., and Zurzolo, C. (2023). Identification and Characterization of Tunneling Nanotubes for Intercellular Trafficking. Curr. Protoc. *3*, e939. https://doi.org/10.1002/cpz1.939.

15. Cordero Cervantes, D., and Zurzolo, C. (2021). Peering into tunneling nanotubes-The path forward. EMBO J. *40*, e105789. https://doi.org/10.15252/embj.2020105789.

16. Pinto, G., Saenz-de-Santa-Maria, I., Chastagner, P., Perthame, E., Delmas, C., Toulas, C., Moyal-Jonathan-Cohen, E., Brou, C., and Zurzolo, C. (2021). Patient-derived glioblastoma stem cells transfer mitochondria through tunneling nanotubes in tumor organoids. Biochem. J. *478*, 21–39. https://doi.org/10.1042/BCJ20200710.

17. Elenbaas, B., Spirio, L., Koerner, F., Fleming, M.D., Zimonjic, D.B., Donaher, J.L., Popescu, N.C., Hahn, W.C., and Weinberg, R.A. (2001). Human breast cancer cells generated by oncogenic transformation of primary mammary epithelial cells. Genes Dev. *15*, 50–65. https://doi.org/10.1101/gad.828901.

18. Sapkota, G., Alarcón, C., Spagnoli, F.M., Brivanlou, A.H., and Massagué, J. (2007). Balancing BMP signaling through integrated inputs into the Smad1 linker. Mol. Cell *25*, 441–454. https://doi.org/10.1016/j.molcel.2007.01.006.

19. Inui, M., Manfrin, A., Mamidi, A., Martello, G., Morsut, L., Soligo, S., Enzo, E., Moro, S., Polo, S., Dupont, S., et al. (2011). USP15 is a deubiquitylating enzyme for receptor-activated SMADs. Nat. Cell Biol. *13*, 1368–1375. https://doi.org/10.1038/ncb2346.

20. Wen, H.-C., Avivar-Valderas, A., Sosa, M.S., Girnius, N., Farias, E.F., Davis, R.J., and Aguirre-Ghiso, J.A. (2011). p38α Signaling Induces Anoikis and Lumen Formation During Mammary Morphogenesis. Sci. Signal. *4*, ra34. https://doi.org/10.1126/scisignal.2001684.

21. Fischbach, N.A., Rozenfeld, S., Shen, W., Fong, S., Chrobak, D., Ginzinger, D., Kogan, S.C., Radhakrishnan, A., Le Beau, M.M., Largman, C., et al. (2005). HOXB6 overexpression in murine bone marrow immortalizes a myelomonocytic precursor in vitro and causes hematopoietic stem cell expansion and acute myeloid leukemia in vivo. Blood *105*, 1456–1466. https://doi.org/10.1182/blood-2004-04-1583.

22. Ouyang, J., Liu, Z., Yuan, X., Long, C., Chen, X., Wang, Y., Liu, L., Liu, S., and Liang, H. (2021). LncRNA PRNCR1 Promotes Breast Cancer Proliferation and Inhibits Apoptosis by Modulating microRNA-377/CCND2/MEK/MAPK Axis. Arch. Med. Res. *52*, 471–482. https://doi.org/10.1016/j.arcmed.2021.01.007.

23. He, M., Jin, Q., Chen, C., Liu, Y., Ye, X., Jiang, Y., Ji, F., Qian, H., Gan, D., Yue, S., et al. (2019). The miR-186-3p/EREG axis orchestrates tamoxifen resistance and aerobic

glycolysis in breast cancer cells. Oncogene *38*, 5551–5565. https://doi.org/10.1038/s41388-019-0817-3.

24. Wang, Y., Cui, J., Sun, X., and Zhang, Y. (2011). Tunneling-nanotube development in astrocytes depends on p53 activation. Cell Death Differ. *18*, 732–742. https://doi.org/10.1038/cdd.2010.147.

25. Nakhle, J., Khattar, K., Özkan, T., Boughlita, A., Abba Moussa, D., Darlix, A., Lorcy, F., Rigau, V., Bauchet, L., Gerbal-Chaloin, S., et al. (2023). Mitochondria Transfer from Mesenchymal Stem Cells Confers Chemoresistance to Glioblastoma Stem Cells through Metabolic Rewiring. Cancer Res. Commun. *3*, 1041–1056. https://doi.org/10.1158/2767-9764.CRC-23-0144.

26. Huang, H., Lu, D., Li, K., Zheng, M., Qin, X., Cui, X., Chen, Y., Chen, C., Huang, N., Zheng, L., et al. (2023). Hsa_circ_0007031 promotes the proliferation and migration of osteosarcoma cells by sponging miR-196a-5p to regulate the HOXB6. Biochem. Pharmacol. *214*, 115667. https://doi.org/10.1016/j.bcp.2023.115667.

27. Vider, B.Z., Zimber, A., Chastre, E., Gespach, C., Halperin, M., Mashiah, P., Yaniv, A., and Gazit, A. (2000). Deregulated expression of homeobox-containing genes, HOXB6, B8, C8, C9, and Cdx-1, in human colon cancer cell lines. Biochem. Biophys. Res. Commun. *272*, 513–518. https://doi.org/10.1006/bbrc.2000.2804.

28. Ding, Z.-Y., Li, R., Zhang, Q.-J., Wang, Y., Jiang, Y., Meng, Q.-Y., Xi, Q.-L., and Wu, G.-H. (2019). Prognostic role of cyclin D2/D3 in multiple human malignant neoplasms: A systematic review and meta-analysis. Cancer Med. *8*, 2717–2729. https://doi.org/10.1002/cam4.2152.

29. Zhong, H., Yang, J., Zhang, B., Wang, X., Pei, L., Zhang, L., Lin, Z., Wang, Y., and Wang, C. (2018). LncRNA GACAT3 predicts poor prognosis and promotes cell proliferation in breast cancer through regulation of miR-497/CCND2. Cancer Biomark. Sect. Dis. Markers *22*, 787–797. https://doi.org/10.3233/CBM-181354.

30. Abba, M.C., Canzoneri, R., Gurruchaga, A., Lee, J., Tatineni, P., Kil, H., Lacunza, E., and Aldaz, C.M. (2020). LINC00885 a Novel Oncogenic Long Non-Coding RNA Associated with Early Stage Breast Cancer Progression. Int. J. Mol. Sci. *21*, 7407. https://doi.org/10.3390/ijms21197407.

31. Hirschhorn, T., Levi-Hofman, M., Danziger, O., Smorodinsky, N.I., and Ehrlich, M. (2017). Differential molecular regulation of processing and membrane expression of Type-I BMP receptors: implications for signaling. Cell. Mol. Life Sci. CMLS *74*, 2645–2662. https://doi.org/10.1007/s00018-017-2488-y.

32. Reindl, J., Shevtsov, M., Dollinger, G., Stangl, S., and Multhoff, G. (2019). Membrane Hsp70-supported cell-to-cell connections via tunneling nanotubes revealed by live-cell STED nanoscopy. Cell Stress Chaperones *24*, 213–221. https://doi.org/10.1007/s12192-018-00958-w.

33. Thayanithy, V., Babatunde, V., Dickson, E.L., Wong, P., Oh, S., Ke, X., Barlas, A., Fujisawa, S., Romin, Y., Moreira, A.L., et al. (2014). Tumor exosomes induce tunneling nanotubes in lipid raft-enriched regions of human mesothelioma cells. Exp. Cell Res. *323*, 178–188. https://doi.org/10.1016/j.yexcr.2014.01.014.

34. Li, Y.C., Park, M.J., Ye, S.-K., Kim, C.-W., and Kim, Y.-N. (2006). Elevated levels of cholesterol-rich lipid rafts in cancer cells are correlated with apoptosis sensitivity induced by cholesterol-depleting agents. Am. J. Pathol. *168*, 1107–1118; quiz 1404–1405. https://doi.org/10.2353/ajpath.2006.050959.

35. Gamell, C., Osses, N., Bartrons, R., Rückle, T., Camps, M., Rosa, J.L., and Ventura, F. (2008). BMP2 induction of actin cytoskeleton reorganization and cell migration requires PI3-kinase and Cdc42 activity. J. Cell Sci. *121*, 3960–3970. https://doi.org/10.1242/jcs.031286.

36. Ishida, H., Jensen, K.V., Woodman, A.G., Hyndman, M.E., and Vogel, H.J. (2017). The Calcium-Dependent Switch Helix of L-Plastin Regulates Actin Bundling. Sci. Rep. *7*, 40662. https://doi.org/10.1038/srep40662.

37. Lin, C.S., Park, T., Chen, Z.P., and Leavitt, J. (1993). Human plastin genes. Comparative gene structure, chromosome location, and differential expression in normal and neoplastic cells. J. Biol. Chem. *268*, 2781–2792.

38. Riplinger, S.M., Wabnitz, G.H., Kirchgessner, H., Jahraus, B., Lasitschka, F., Schulte, B., van der Pluijm, G., van der Horst, G., Hämmerling, G.J., Nakchbandi, I., et al. (2014). Metastasis of prostate cancer and melanoma cells in a preclinical in vivo mouse model is enhanced by L-plastin expression and phosphorylation. Mol. Cancer *13*, 10. https://doi.org/10.1186/1476-4598-13-10.

39. Janji, B., Vallar, L., Al Tanoury, Z., Bernardin, F., Vetter, G., Schaffner-Reckinger, E., Berchem, G., Friederich, E., and Chouaib, S. (2010). The actin filament cross-linker L-plastin confers resistance to TNF-alpha in MCF-7 breast cancer cells in a phosphorylation-dependent manner. J. Cell. Mol. Med. *14*, 1264–1275. https://doi.org/10.1111/j.1582-4934.2009.00918.x.

40. Machado, R.A.C., Stojevski, D., De Landtsheer, S., Lucarelli, P., Baron, A., Sauter, T., and Schaffner-Reckinger, E. (2021). L-plastin Ser5 phosphorylation is modulated by the PI3K/SGK pathway and promotes breast cancer cell invasiveness. Cell Commun. Signal. CCS *19*, 22. https://doi.org/10.1186/s12964-021-00710-5.

41. Delage, E., Cervantes, D.C., Pénard, E., Schmitt, C., Syan, S., Disanza, A., Scita, G., and Zurzolo, C. (2016). Differential identity of Filopodia and Tunneling Nanotubes revealed by the opposite functions of actin regulatory complexes. Sci. Rep. *6*, 39632. https://doi.org/10.1038/srep39632.

42. Dawson, P.J., Wolman, S.R., Tait, L., Heppner, G.H., and Miller, F.R. (1996). MCF10AT: a model for the evolution of cancer from proliferative breast disease. Am. J. Pathol. *148*, 313–319.

43. Kim, S.-J., Saeidi, S., Cho, N.-C., Lee, H.-B., Han, W., Kim, K.P., and Surh, Y.-J. (2025). Cooperation between oncogenic NRF2 and wild-type HRAS promotes progression of breast cancer. Cell. Signal. *134*, 111920. https://doi.org/10.1016/j.cellsig.2025.111920.

44. Romieu, I., Scoccianti, C., Chajès, V., de Batlle, J., Biessy, C., Dossus, L., Baglietto, L., Clavel-Chapelon, F., Overvad, K., Olsen, A., et al. (2015). Alcohol intake and breast cancer in the European prospective investigation into cancer and nutrition. Int. J. Cancer *137*, 1921–1930. https://doi.org/10.1002/ijc.29469.

45. Giampiccolo, C., Fervers, B., Coudon, T., Praud, D., Vigneron, A., Grassot, L., Mercoeur, B., Faure, E., Frenoy, P., Génard-Walton, M., et al. (2026). Statistical approaches to analyse the combined effect of seven air pollutants and breast cancer risk: a case–control study nested in the French E3N-Generations cohort. BMC Med. *24*, 112. https://doi.org/10.1186/s12916-026-04653-x.

46. Clément, F., Xu, X., Donini, C.F., Clément, A., Omarjee, S., Delay, E., Treilleux, I., Fervers, B., Le Romancer, M., Cohen, P.A., et al. (2017). Long-term exposure to bisphenol A or benzo(a)pyrene alters the fate of human mammary epithelial stem cells in response to BMP2 and BMP4, by pre-activating BMP signaling. Cell Death Differ. *24*, 155–166. https://doi.org/10.1038/cdd.2016.107.

47. Korenkova, O., Liu, S., Prlesi, I., Pepe, A., Albadri, S., Del Bene, F., and Zurzolo, C. (2024). Tunneling nanotubes enable intercellular transfer in zebrafish embryos. Dev. Cell, S1534-5807(24)00635-X. https://doi.org/10.1016/j.devcel.2024.10.016.

48. Perez-Riverol, Y., Xu, Q.-W., Wang, R., Uszkoreit, J., Griss, J., Sanchez, A., Reisinger, F., Csordas, A., Ternent, T., Del-Toro, N., et al. (2016). PRIDE Inspector Toolsuite: Moving Toward a Universal Visualization Tool for Proteomics Data Standard Formats and Quality Assessment of ProteomeXchange Datasets. Mol. Cell. Proteomics MCP *15*, 305–317. https://doi.org/10.1074/mcp.O115.050229.

49. Perez-Riverol, Y., Bandla, C., Kundu, D.J., Kamatchinathan, S., Bai, J., Hewapathirana, S., John, N.S., Prakash, A., Walzer, M., Wang, S., et al. (2025). The PRIDE database at 20 years: 2025 update. Nucleic Acids Res. *53*, D543–D553. https://doi.org/10.1093/nar/gkae1011.

553 **Figure Legends.**

554 **Fig. 1** | Structural characterization of TNTs upon mammary cell transformation. A, Schematic
555 of our MCF10A-derived cell lines *(5)*. B, Immunofluorescence images of actin (red) in TNTs,
556 observed by super-resolution Airyscan confocal microscopy with 40x oil objective. Nuclei,
557 Hoechst labeling (blue). Scale bars, 20 μm. C, TNT number (> 8 μm) quantification *per* 100
558 cells (left, n = 9 biological replicates), and % of long TNTs (> 50 μm; right, n = 4 biological
559 replicates). Ten Z-stacks of 10 sections each were taken *per* condition, and 100 cells minimum
560 *per* experiment were counted. TNTs were counted and measured in each Z-stack. Error bars
561 depict SD. P-values were calculated with one-way ANOVA with post-hoc Tukey test (ns, not
562 significant; * $p < 0.05$; ** $p < 0.01$; *** $p < 0.001$). D, Scanning electron microscopy images
563 of TNTs of MCF10A-CT, MC26 and M1B26 cells. Black arrow, TNT bulge. Scale bars
564 MCF10A-CT: 40 and 50 μm; MC26: 50 and 5 μm; M1B26: from left to right: 20, 3, 20, 3 μm.
565 E, Transmission electron microscopy images of an open-ended TNT linking two M1B26 cells,
566 with mitochondria (red asterisks). Scale bars, 5 μm (low mag), 500 nm (high mag). F,
567 Immunofluorescence images of mitochondria (green) in MCF10A-CT and M1B26 cells. Actin,
568 red; nuclei, blue. Scale bars, 20 μm. G, Immunofluorescence images of actin (red) in mammary
569 acini grown from MC26 and M1B26 cells. Scale bars, 5 μm. Right, 3D-projection of a TNT
570 linking two M1B26 cells, obtained with Zeiss ZENlite3.6 software. Actin, red; nuclei, blue. H,
571 Images of TNTs linking M1B26 (GFP, green, and transmitted light) to normal human primary
572 mammary fibroblasts (transmitted light). Nuclei, blue. Scale bars, 20 μm. I, Images of TNTs
573 linking M1B26 (GFP, green) to normal human primary mammary cells. Actin, red; nuclei, blue.
574 Asterisks: emerging from M1B26 (green); between both cell types (red). Scale bars: top, 20
575 μm, bottom, 10 μm.

576

577 **Fig. 2** | TNTs link transformed and non-transformed mammary cells, favoring an horizontal
578 directional transfer of information. A, Fluorescence images of GFP-labeled-M1B26
579 (transformed - Tf; green) and mCherry-labeled MCF10A (non-transformed - NoTf; red) cells,
580 after 48 h in coculture. Scale bars, 5 μm. B,C, Relative number of TNTs linking NoTf to Tf, or
581 Tf to NoTf cells (B) and TNT ratio defined as $\frac{NoTf>Tf}{NoTf-NoTf}$ (black arrows *vs* red lines) or $\frac{Tf>NoTf}{Tf-Tf}$
582 (black arrows *vs* green lines) after 48h in coculture (C). Z stacks of 10 sections each were taken
583 *per* condition and 100 cells minimum were counted. TNTs were counted and measured in each
584 Z-stack. Error bars depict SD. Statistical significance was calculated using an unpaired

585 Student's two-sided t test with Welch's correction (n = 5 biological replicates; *** $p < 0.001$).
586 D, Fluorescence images of material transfer (green dots) from Tf (green) to NoTf cells.
587 Membranes, red; nuclei, blue. Scale bars: 100 μm, in zoom 20 μm. E, Time-lapse snapshots of
588 green material trafficking within a TNT bulge (*), from a (green) Tf to NoTf cells after 48 h in
589 coculture. Membranes, red; nuclei, blue. Scale bar, 100 μm; images recorded for 75 min, with
590 one image every 18 min (see Supplementary Movie 1). F, Flow cytometry analysis of an 8-day
591 coculture of green Tf and red NoTf cells, with a schematic of NoTf accepting material from Tf
592 cells (top: NoTf accept green, red cell with green dots), and Tf cells accepting material from
593 NoTf cells (bottom: Tf accept red, green cell with red dots). G,H, Quantification of the
594 percentage of exchange (G; n = 8 biological replicates) and fluorescence intensity (H; n = 7
595 biological replicates), for indicated transfer. Error bars depict SD. Statistical significance was
596 calculated using an unpaired Student's two-sided t test with Welch's correction (*** $p < 0.001$).
597 I, Schematic of the experimental design of coculture experiments. J,K, Quantification of the
598 number of acceptor cells *per* 10,000 cells (J), and fluorescence intensity (K), in standard or
599 Transwell™ cocultures, for indicated transfer involving normal human primary mammary
600 (normal) and M1B26 cells (Tf). Error bars depict SD. Statistical significance was calculated
601 using an unpaired Student's two-sided t test with Welch's correction (n = 3 biological replicates;
602 ns, not significant; * $p < 0.05$; ** $p < 0.01$).

603

604 **Fig. 3** | TNT-dependent phenotypic changes of non-transformed cells acceptor of material from
605 transformed cells. A, Schematic of the experimental design: 4 cell populations, sorted by flow
606 cytometry (NoTf, Tf, NoTf in coculture without fluorescent transfer [non-transformed non-
607 acceptor cells - NoTf no accept], NoTf in coculture with fluorescent transfer [non-transformed
608 acceptor cells - NoTf accept]), underwent proteomic analyses and RT-qPCR. B,C, Volcano plot
609 (B) showing Log_2 enrichment of individual proteins in NoTf accept compared to NoTf no
610 accept cells from the same coculture (see schematic). P-value threshold was set at 0.05 and 0.8
611 for Log_2 fold change. C, To obtain a larger pool of hits, it was lowered to 0.5, generating a list
612 of 193 proteins upregulated in NoTf accept cells, used to generate the GOBP subset with
613 STRING (https://string-db.org). D,E, Box and whiskers plots of Log_2LFQ values (Protein
614 Levels) of EST1 (*CES1*), Plastin-2 (*LCP1*), Rab-6B (*RAB6B*), TRIQK (*TRIQK*) (D), and H-
615 Ras and K-Ras (E), for indicated sorted cell populations. Statistical significance was calculated
616 using one-way ANOVA with Dunnett's multiple comparison test (n = 5 biological replicates; *
617 $p < 0.05$; ** $p < 0.01$; *** $p < 0.001$; **** $p < 0.0001$). For clarity, comparisons with Tf cells

618 were omitted, and in (E), only significant comparison are shown. F,G, Immunofluorescence
619 images of actin (red) and tubulin (green) in (F) HMLE and HMLER cells, and (G) MCF10A,
620 MCF10.AT1 and MCF10.DCIS cells. Nuclei, blue. Scale bars = 20 µm. H,I, From left to right:
621 quantification of TNT number *per* cell, average length, and percentage of long TNTs in
622 indicated cell lines. Ten Z-stacks of 10 sections each were taken *per* condition and 100 cells
623 minimum *per* experiment were counted. TNTs were counted and measured in each Z-stack.
624 Statistical significance was calculated using an unpaired Student's two-sided t test with Welch's
625 correction (n = 8 and n = 5 biological replicates for HMEC-derived and MCF10A-derived cell
626 lines, respectively; ns, not significant; ** $p < 0.01$).

627

628 **Fig. 4** | Expression of actors of the BMP signaling pathway is enhanced in acceptor cells after
629 TNT transfer. A, Box and whiskers plots of Log_2LFQ values (Protein Levels) of ID1, Nup214,
630 Spartin, USP15, ATF2, MAPKAPK2 and Rac1, for indicated sorted cell populations. Statistical
631 significance was calculated using one-way ANOVA with Dunnett's multiple comparison test (n
632 = 5 biological replicates; * $p < 0.05$; ** $p < 0.01$; *** $p < 0.001$; **** $p < 0.0001$). For clarity,
633 only comparison between NoTf and NoTf accept cells is shown. B, Immunofluorescence
634 images of actin (red) and BMPR1b (green) in indicated cells. Nuclei (blue). Scale bars, 20 µm.
635 C, Correlative light scanning electron microscopy (SEM) of BMPR1b, immunostained with
636 Alexa Fluor®488-Fluoronanogold™ (green) in M1B26 cells. From left to right: Airyscan
637 confocal, scanning electron microscopy, zooms, correlative (overlay). Scale bars, 10 µm, unless
638 otherwise indicated. D, Immunofluorescence of actin (green), after transfection with siRNA
639 pools targeting *BMPR1b* (siBMPR1b) or *GPER* (siGPER). Non-targeting siRNA: siCTRL. E,
640 *BMPR1B* and *GPER* transcript and protein expression upon their silencing (top),with siCTRL
641 set at 1 (n = 4), and (bottom) TNT number (> 8 µm) *per* cell and % of long TNTs (> 50 µm)
642 upon indicated silencing, normalized against siCTRL. Error bars depict SD. Statistical
643 significance was calculated using an unpaired Student's two-sided t test with Welch's correction
644 (n = 4 biological replicates, *** $p < 0.001$). F, Schematic of experimental design: after sorting,
645 cell populations were either lysed and subjected to RT-qPCR for selected transcript analyses, or
646 grown for several weeks with or without BMP2/IL6, and immunoblot analyses performed at
647 end points. G, RT-qPCR measurement of BMPR1b mRNA in indicated cell populations, the
648 expression in NoTf cells (monocultures) set at 1. Statistical significance was calculated using
649 one-way ANOVA with post-hoc Tukey test (n = 5 biological replicates). For clarity, only
650 comparison between NoTf accept and NoTf cells is shown (**** $p < 0.0001$).

651 **Fig. 5** | Non-transformed cells acceptor of information from transformed cells *via* TNTs
652 display preneoplastic features. A, Left, quantification of BMPR1b immunoblots performed on
653 NoTf accept cells grown in the presence of BMP2/IL6, for indicated weeks post sorting. Box
654 and whiskers plot of 6 biological replicates. Statistical significance was calculated using a one-
655 way ANOVA with non-parametric Kruskal-Wallis test, and for clarity, only p-values ≤ 0.05 are
656 indicated. Right, quantification of BMPR1b immunoblots performed on indicated cells, 14
657 weeks post sorting, with NoTf conditions set at 1 (n = 6 biological replicates). Statistical
658 significance was calculated using a one-way ANOVA with post-hoc Tukey test (*** p < 0.001).
659 B,C, Quantification of p-SMAD1/5/8 / SMAD1/5/8 (B) and p-p38/p38 (C) immunoblots
660 performed on NoTf accept cells grown in the presence of BMP2/IL6, for indicated weeks post
661 sorting. Box and whiskers plot of 6 biological replicates. Statistical significance was calculated
662 using a one-way ANOVA with non-parametric Kruskal-Wallis test, and for clarity, only p-values
663 ≤ 0.05 are indicated. D, RNA-sequencing results of transcriptomic expression levels of *HOXB6,*
664 *CCND2, EREG* and *HRAS* in indicated cell lines (n = 3 biological replicates). Data deposited
665 on the Gene Expression Omnibus repository, GSE186734 *(5)*. Error bars depict SD. Statistical
666 significance was calculated using a one-way ANOVA with post-hoc Tukey test (* p < 0.05; **
667 p < 0.01; *** p < 0.001; **** p < 0.0001). E, RT-qPCR measurements of HOXB6, CCND2,
668 EREG and HRAS mRNA in indicated cell populations, with the expression in NoTf cells set at
669 to 1. Error bars depict SD. Statistical significance was calculated using a one-way ANOVA with
670 post-hoc Tukey test (biological replicates: n = 8 for *HOXB6*, n = 5 for *CCND2*, n = 7 for *EREG*,
671 n = 8 for *HRAS*). For clarity, only comparisons between NoTf, NoTf Transwell and NoTf accept
672 cells are shown (* p < 0.05; ** p < 0.01; *** p < 0.001; **** p < 0.0001). F, Quantification of
673 soft agar clones of indicated sorted cells, after 8, 10, 14 and 16 weeks in culture with or without
674 BMP2/IL6 (n = 3 biological replicates). Error bars represent SD. Statistical significance was
675 calculated using a one-way Welch and Brown-Forsythe ANOVA test (* p < 0.05; ** p < 0.01;
676 *** p < 0.001; **** p < 0.0001). For clarity, only p-values ≤ 0.05 are indicated, and
677 comparisons with Tf cells are omitted. G, Model depicting how TNTs might be involved in the
678 propagation of a BMP-dependent preneoplastic state. Fibrils and fibers illustrate extracellular
679 matrix components.
680

Cuella Martin *et al* Figure 1

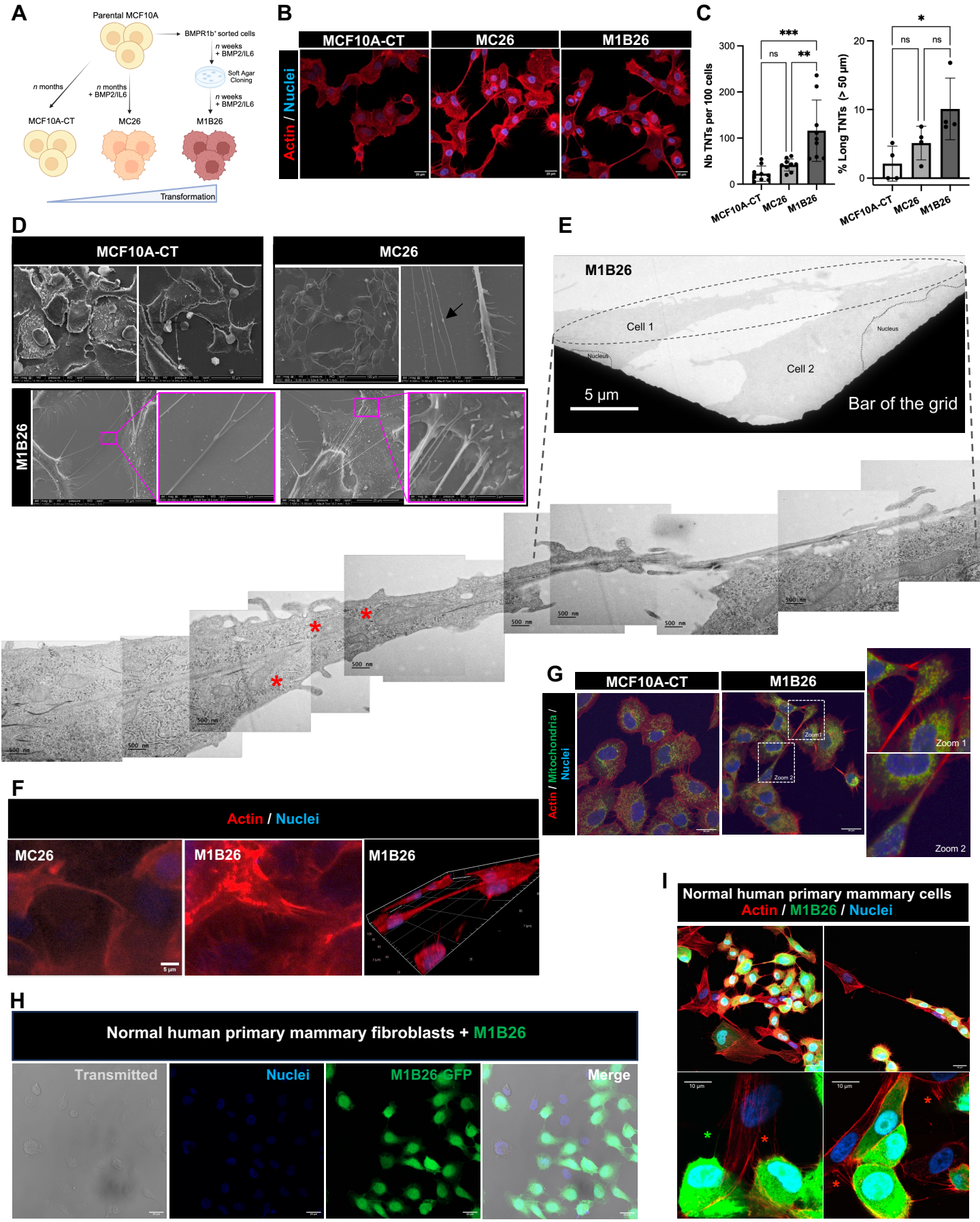

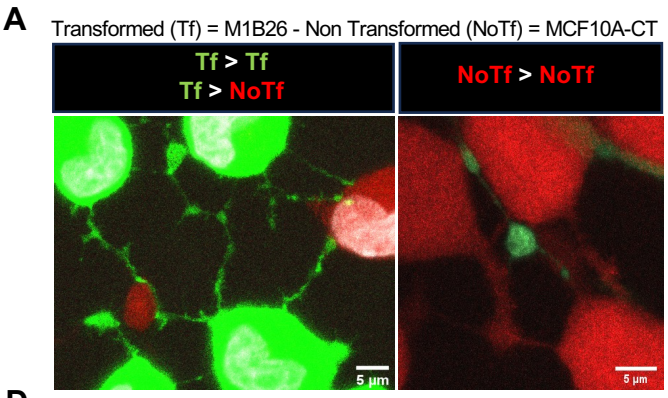

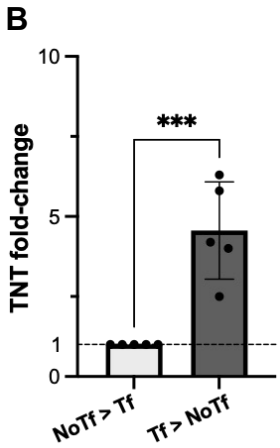

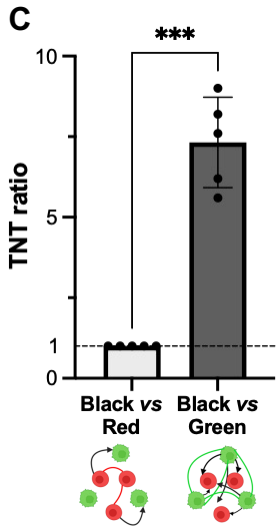

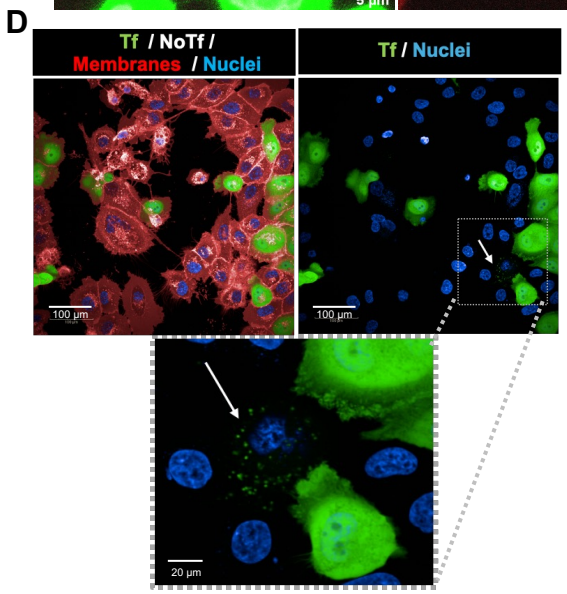

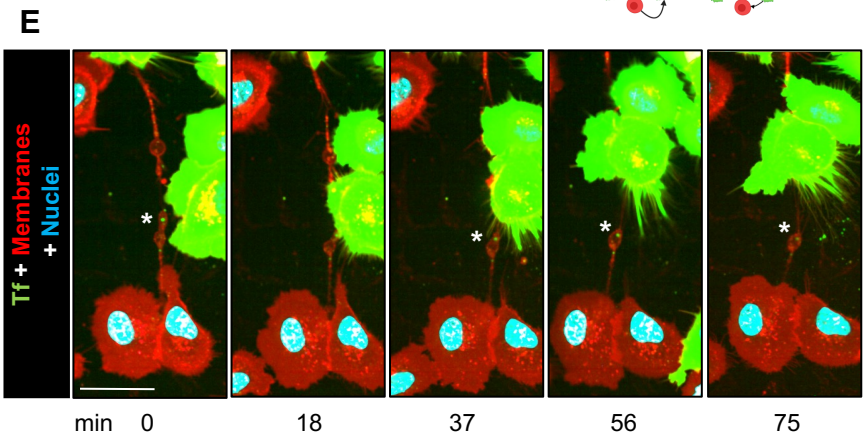

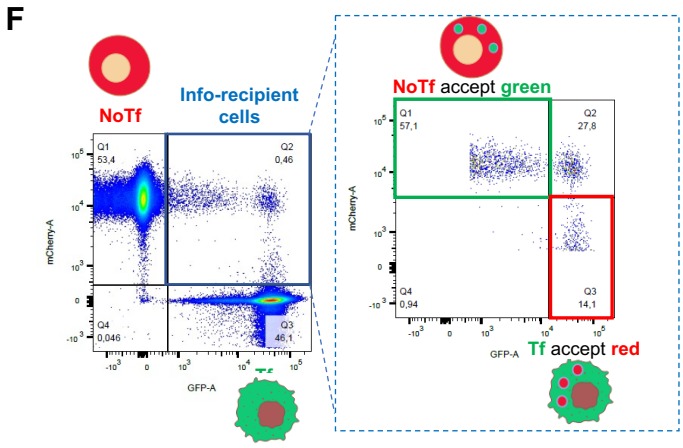

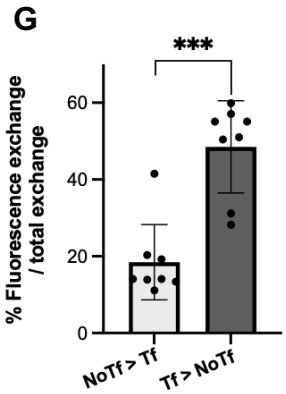

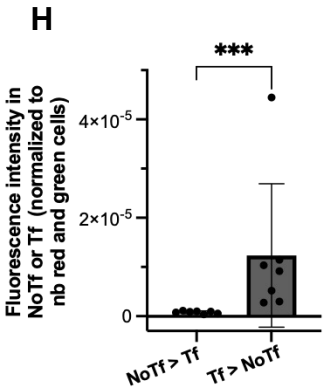

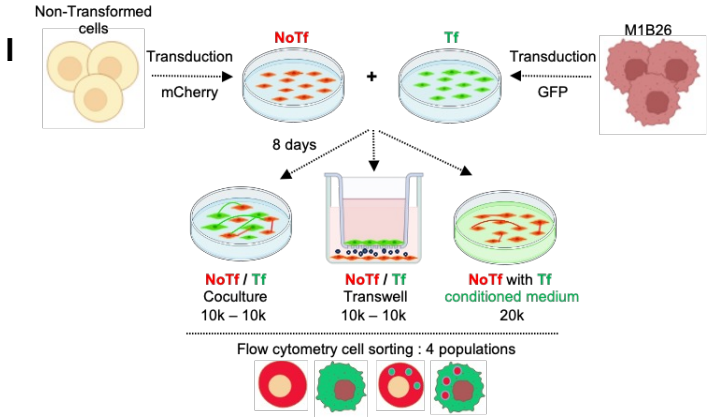

NoTf = Normal human primary mammary cells

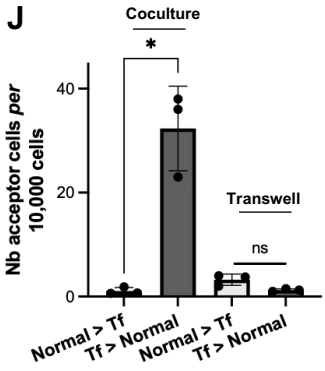

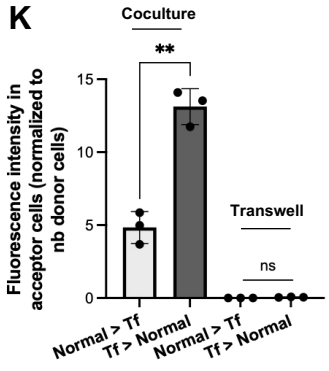

Cuella Martin *et al* Figure 3

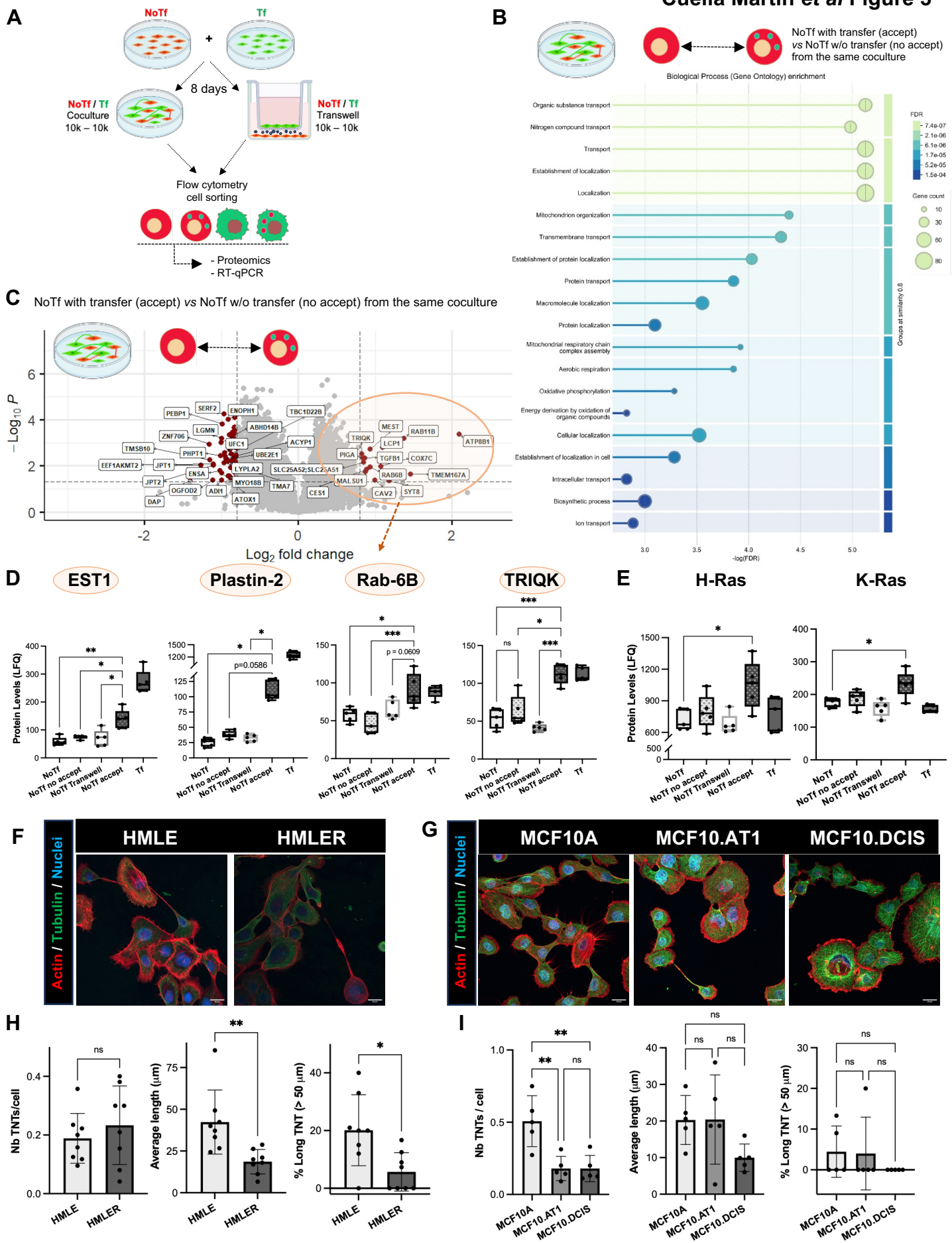

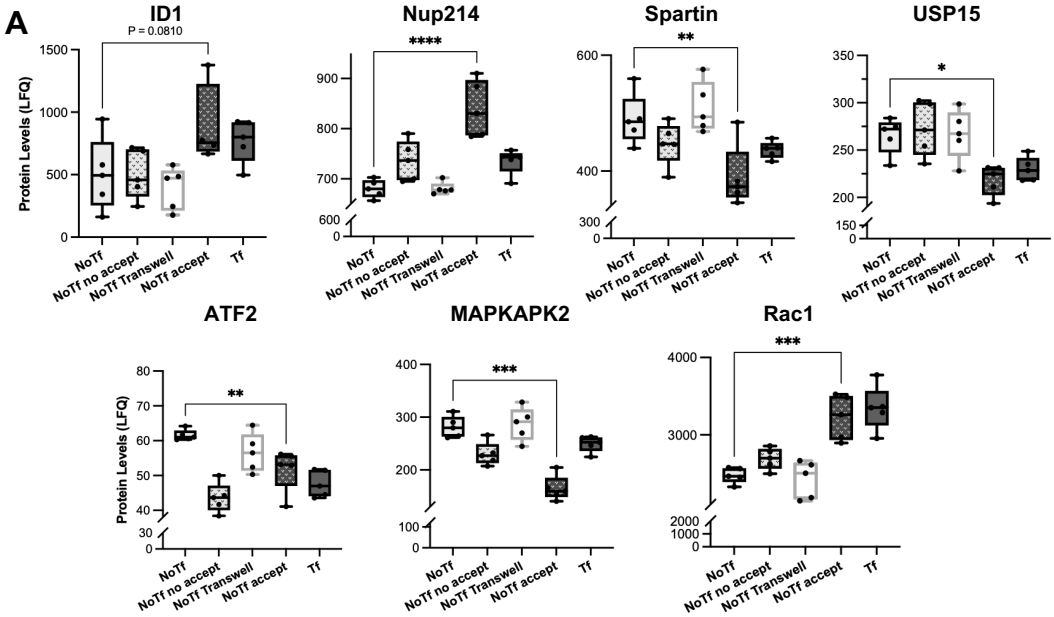
A
ID1
P = 0.0810
Nup214
****
Spartin
**
USP15
*
ATF2
**
MAPKAPK2
***
Rac1
***
Protein Levels (LFQ)
NoTf
NoTf no accept
NoTf Transwell
NoTf accept
Tf

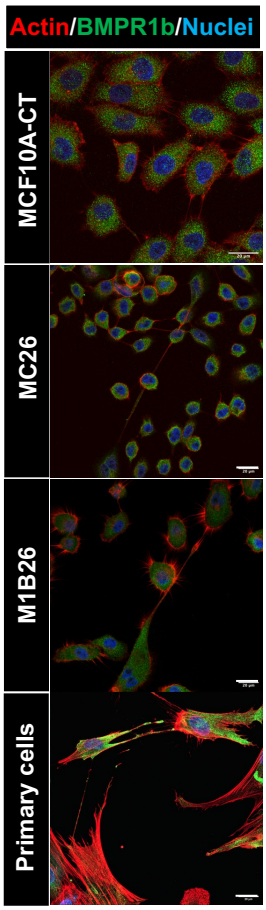
B
Actin/BMPR1b/Nuclei
MCF10A-CT
MC26
M1B26
Primary cells

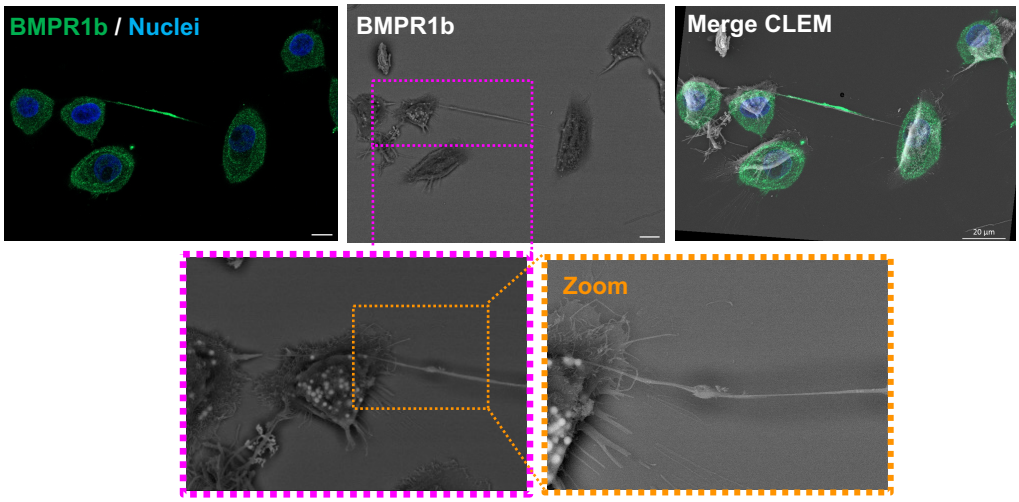
C
BMPR1b / Nuclei
BMPR1b
Merge CLEM
Zoom

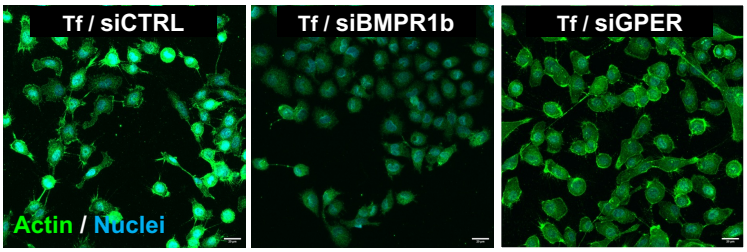
D
Tf / siCTRL
Tf / siBMPR1b
Tf / siGPER
Actin / Nuclei

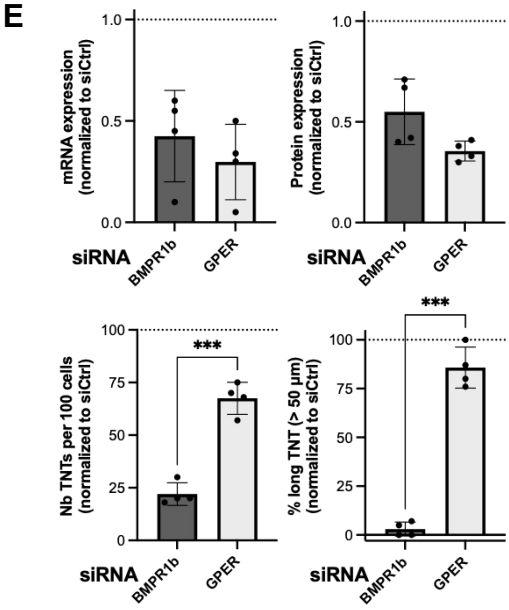
E
mRNA expression (normalized to siCtrl)
Protein expression (normalized to siCtrl)
Nb TNTs per 100 cells (normalized to siCtrl)
% long TNT (> 50 µm) (normalized to siCtrl)
siRNA
BMPR1b
GPER
***

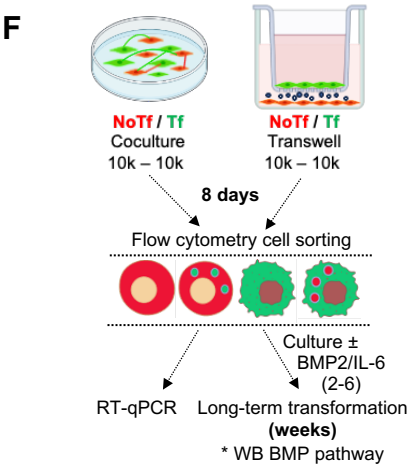
F
NoTf / Tf
Coculture
10k – 10k
NoTf / Tf
Transwell
10k – 10k
8 days
Flow cytometry cell sorting
Culture ±
BMP2/IL-6
(2-6)
RT-qPCR
Long-term transformation
(weeks)
* WB BMP pathway

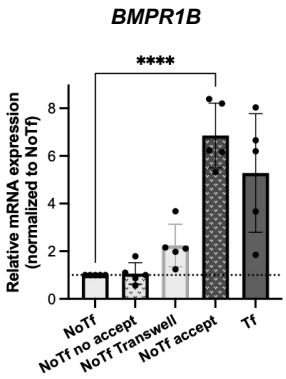
G
BMPR1B
****
Relative mRNA expression (normalized to NoTf)
NoTf
NoTf no accept
NoTf Transwell
NoTf accept
Tf

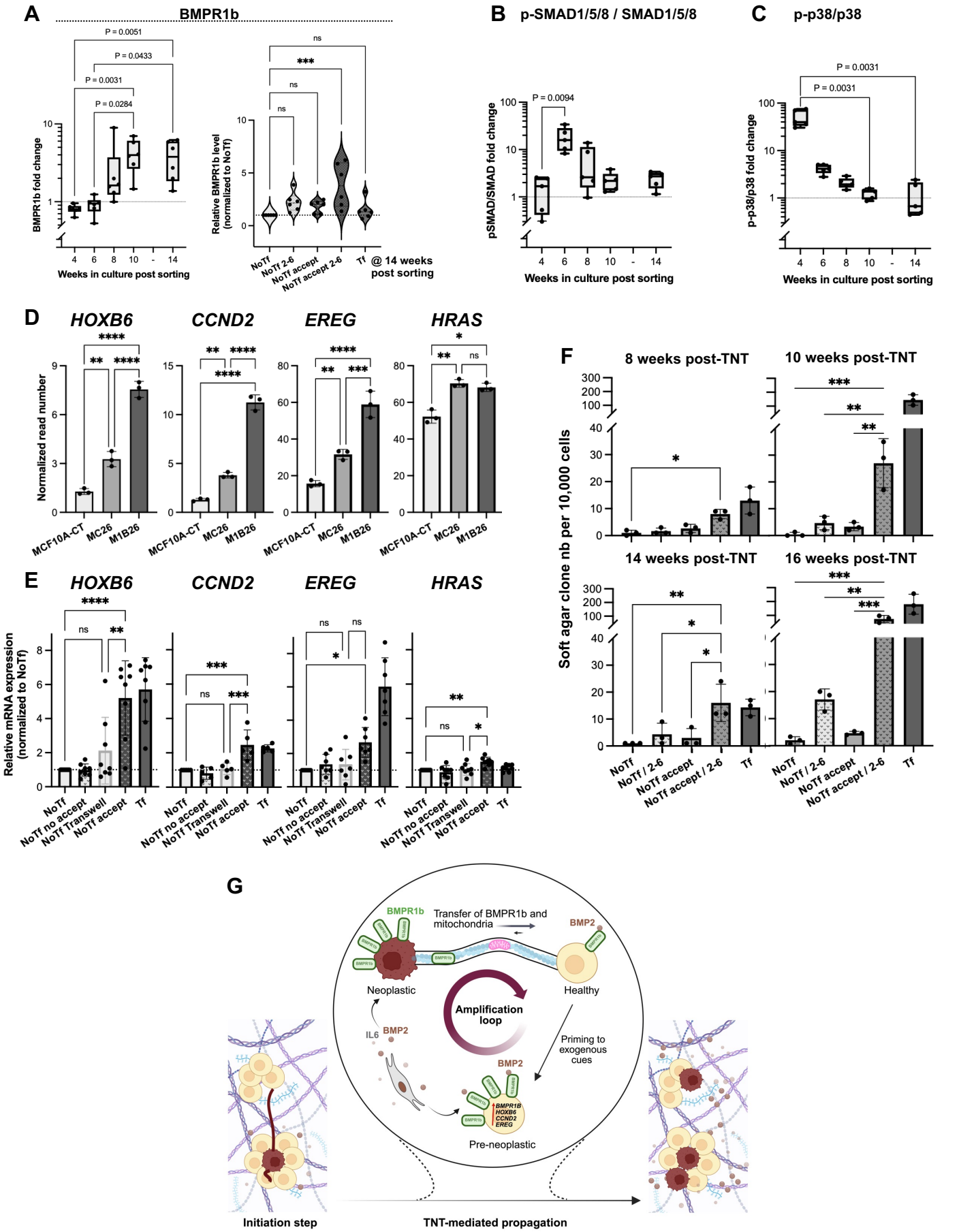
A
BMPR1b
P = 0.0051
P = 0.0433
P = 0.0031
P = 0.0284
BMPR1b fold change
Weeks in culture post sorting
ns
***
ns
ns
Relative BMPR1b level (normalized to NoTf)
NoTf
NoTf 2-6
NoTf accept
NoTf accept 2-6
Tf
@ 14 weeks post sorting
B
p-SMAD1/5/8 / SMAD1/5/8
P = 0.0094
pSMAD/SMAD fold change
Weeks in culture post sorting
C
p-p38/p38
P = 0.0031
P = 0.0031
p-p38/p38 fold change
Weeks in culture post sorting
D
HOXB6
CCND2
EREG
HRAS
Normalized read number
MCF10A-CT
MC26
M1B26
E
HOXB6
CCND2
EREG
HRAS
Relative mRNA expression (normalized to NoTf)
NoTf
NoTf no accept
NoTf Transwell
NoTf accept
Tf
F
8 weeks post-TNT
10 weeks post-TNT
14 weeks post-TNT
16 weeks post-TNT
Soft agar clone nb per 10,000 cells
NoTf
NoTf / 2-6
NoTf accept
NoTf accept / 2-6
Tf
G
BMPR1b
Transfer of BMPR1b and mitochondria
BMP2
Neoplastic
Healthy
Amplification loop
IL6
BMP2
Priming to exogenous cues
BMP2
BMPR1B
HOXB6
CCND2
EREG
Pre-neoplastic
Initiation step
TNT-mediated propagation